

# Hypernuclear and $\Lambda$ -spin polarizations produced in the $(\pi^+, K^+)$ reaction

K. Itonaga

*Laboratory of Physics, Miyazaki Medical College, Kiyotake, Miyazaki 889-16, Japan*

T. Motoba

*Laboratory of Physics, Osaka Electro-Communication University, Neyagawa, Osaka 572, Japan*

O. Richter\* and M. Sotona

*Nuclear Physics Institute, Czech Academy of Sciences, 250 68 Řež/Prague, Czech Republic*

(Received 28 June 1993)

Starting with the elementary amplitudes having spin-flip and spin-nonflip interactions for  $\pi^+n \rightarrow \Lambda K^+$ , hypernuclear production cross sections and polarizations have been estimated in detail for the  $(\pi^+, K^+)$  reaction on available  $p$ -shell nuclear targets ( $^{10,11}\text{B}$ ,  $^{12,13}\text{C}$ ,  $^{14}\text{N}$ ,  $^{16}\text{O}$ ). The experimental excitation spectra of  $^{\Lambda}_{12}\text{C}$ ,  $^{\Lambda}_{13}\text{C}$ , and  $^{\Lambda}_{16}\text{O}$ , including the typical cross section data, are satisfactorily reproduced in the distorted wave impulse approximation with the configuration-mixed wave functions. The angular dependence of hypernuclear polarization is predicted for each typical state, showing, for example, that the use of the mixed wave functions changes appreciably the previous estimate with the simple one-particle-one-hole wave function for  $^{\Lambda}_{12}\text{C}$ . The  $\Lambda$ -spin polarization in nuclear medium is also estimated. Typical states are shown to have large polarizations at the hypernuclear production stage.

PACS number(s): 21.80.+a, 24.70.+s, 25.80.Hp

## I. INTRODUCTION

The production of hypernuclear polarization is an interesting subject, providing us a possibility to investigate the detailed spectroscopy, hypernuclear weak decays, and the magnetic moment of a  $\Lambda$  hyperon in the nuclear medium [1,2]. Masaïke and Ejiri [3] have discussed a possible measurement of the hypernuclear polarization. The theoretical study was first made in Refs. [4,5] in which, however, the calculation was limited to the absorption-based polarization without any spin-flip interaction. It is known experimentally that the elementary  $\pi^-p \rightarrow \Lambda K^0$  process at  $p_{\pi^-} \simeq 1 \text{ GeV}/c$  produces large and positive polarization of the  $\Lambda$  hyperon [6]. Therefore, the charge conjugate  $\pi^+n \rightarrow \Lambda K^+$  process is also expected to polarize the hyperon. The elementary amplitudes for this process were reanalyzed by Žofka and one of the authors (M.S.) [7], providing the spin-nonflip and spin-flip amplitudes in a convenient form. Starting with these elementary amplitudes, the calculational procedure to treat hypernuclear polarizations in  $(\pi^+, K^+)$  has been formulated in Ref. [8].

Recently, the ECHO group performed the  $(\pi^+, K^+)$  coincidence experiment on the deuteron and  $^{12}\text{C}$  targets at KEK [9]. They measured the asymmetry of the weak decay particles and also the polarization of a  $\Lambda$  hyperon in the quasifree region, providing interesting information on the polarization of hypernuclei. It should be noted, how-

ever, that one has to separate the physical process into two stages in order to discuss theoretical and experimental hypernuclear polarizations. First, at the *production stage*, we have to estimate both the cross section and the polarization of each hypernuclear state as a direct result of the  $(\pi^+, K^+)$  reaction. Then subsequent decays of hypernuclear excited states occur by emitting  $\gamma$ , a nucleon and/or nuclear clusters. Thus the ground-state polarization should be modified by these depolarization effects before going to decay by the weak interaction. The amount of polarization at this *weak decay stage* plays the crucial role in elucidating the nonmesonic decay mechanism to which much attention has been paid in recent years.

In order to meet the improved coincidence experiments in the near future, we aim to get careful predictions of hypernuclear polarizations at both stages mentioned above. Here we are concerned with the physical quantities at the production stage, and in the subsequent paper we will take the depolarization processes into account to get the polarization at the weak decay stage. In this paper the cross sections and polarizations in the  $(\pi^+, K^+)$  reaction for some interesting  $p$ -shell targets ( $^{10,11}\text{B}$ ,  $^{12,13}\text{C}$ ,  $^{14}\text{N}$ , and  $^{16}\text{O}$ ) are calculated within the framework of the distorted wave impulse approximation (DWIA). The novelty of this paper is to present such estimates obtained by combining the configuration-mixed shell-model wave functions with the elementary interaction having spin-flip and spin-nonflip amplitudes. It is noted that Ref. [8] employed the single one-particle-one-hole (1p-1h) hypernuclear wave function ( $j_n^{-1}j_\Lambda$ ) to demonstrate polarizations of typical states (in  $^{\Lambda}_{12}\text{C}$  within the  $p$ -shell region). The hypernuclear polarization may be rather sensitive

\*Present address: Gramofonové Závody, 26712 Loděnice, Czech Republic.

to the adopted wave functions. Thus it is interesting to compare such simple estimates with the values obtained here by using the refined wave function. We also estimate the  $\Lambda$ -spin polarization in nuclei which is relevant to the nonmesonic decay.

As far as the  $(\pi^+, K^+)$  excitation functions are concerned, there have been several extensive calculations [10–14], which should correspond to a series of the  $(\pi^+, K^+)$  experiments [15–18]. Although these calculations were successful in predicting or explaining the main feature of the reaction, all of the authors employed a prescription of the standard approximation,

$$\frac{d\sigma}{d\Omega} = \alpha \left( \frac{d\sigma}{d\Omega} \right)_{\pi n \rightarrow \Lambda K}^{\text{EXP}} N_{\text{eff}},$$

instead of starting with the elementary amplitudes. This approximation corresponds to neglecting the elementary spin-flip amplitude. Therefore, it is also interesting to compare the new estimates with the previous ones of Ref. [14] in which the same wave functions were employed but the cross section was given by the prescription.

In the following, Sec. II is devoted to summarize the calculational procedure including the description of the nuclear and hypernuclear wave functions. In Sec. III the calculated cross sections and excitation functions are presented together with the comparison with the available data ( ${}_{\Lambda}^{12}\text{C}$ ,  ${}_{\Lambda}^{13}\text{C}$ , and  ${}_{\Lambda}^{16}\text{O}$ ). In Sec. IV we discuss the hypernuclear polarizations and the  $\Lambda$ -spin polarizations at the production stage. Concluding remarks are given in Sec. V.

## II. OUTLINE OF THE CALCULATION

### A. Cross section and polarization

On the basis of the elementary amplitudes for  $\pi^+ n \rightarrow \Lambda K^+$ , the Hamiltonian used to describe the  ${}^A Z(a, b)_{\Lambda}^A Z$  reaction can be written in DWIA as follows, with  $a$  and  $b$  denoting  $\pi^+$  and  $K^+$ , respectively:

$$\hat{O} = \int d\mathbf{r} \left[ \chi^{(-)*} \left( \mathbf{p}_b, \frac{M_A}{M_H} \mathbf{r} \right) \chi^{(+)} (\mathbf{p}_a, \mathbf{r}) \right] \\ \times \sum_{j=1}^A U_-(j) \delta \left( \mathbf{r} - \frac{M_C}{M_A} \mathbf{r}_j \right) [f + ig(\boldsymbol{\sigma}_j \cdot \hat{\mathbf{n}})]. \quad (1)$$

Here  $\chi$ 's are meson distorted waves and the operator  $U_-$  converts a neutron into a  $\Lambda$  hyperon.  $\hat{\mathbf{n}}$  is a unit vector perpendicular to the reaction plane and  $\boldsymbol{\sigma}_j$  is the baryon spin operator.  $M$ 's are the nuclear and hypernuclear masses and the core mass of the hypernucleus participating in the reaction.  $f$  and  $g$  denote the elementary amplitudes for the spin-nonflip and spin-flip interactions, respectively [7]. Here we outline only the basic formulas briefly for the sake of completeness, since one may refer to Ref. [8] for the detailed expressions.

The polarization is calculated in the coordinate frame  $S_2$  defined as follows:

$\{S_2\}$  frame :

$$\hat{\mathbf{z}} = \hat{\mathbf{n}} = \frac{\mathbf{p}_a \times \mathbf{p}_b}{|\mathbf{p}_a \times \mathbf{p}_b|}, \quad \hat{\mathbf{y}} = \hat{\mathbf{p}}_a, \quad \hat{\mathbf{x}} = \hat{\mathbf{y}} \times \hat{\mathbf{z}}, \quad (2)$$

where  $\mathbf{p}_a$  ( $\mathbf{p}_b$ ) represents the incoming (outgoing) meson momentum.

Every necessary quantity is expressed in terms of the basic transition matrix element  $R(fi; M_f)$  which is defined with initial and final state wave functions by

$$R(fi; M_f) = \frac{1}{[J_i]} \sum_{M_i} \left| \langle J_f M_f T_f \tau_f | \hat{O} | J_i M_i T_i \tau_i \rangle \right|^2. \quad (3)$$

One should note here that a projection  $M_f$  of the final state angular momentum is kept explicitly. Then the cross section in the laboratory frame is expressed as

$$\frac{d\sigma}{d\Omega}(\theta_L) = \frac{(2\pi)^4 p_b^2 E_a E_b E_H}{p_a [p_b(E_H + E_b) - p_a E_b \cos \theta_L]} \\ \times \lambda^2 \sum_{M_f} R(fi; M_f), \quad (4)$$

where  $p$ 's and  $E$ 's are the momenta and the energies in the  $A$ -body laboratory frame, respectively.  $E_H$  is the energy of the produced hypernucleus. The factor  $\lambda$  stems from the two-body center of mass and two-body laboratory frame transformation, because elementary amplitudes are usually given in the two center of mass frame. This factor is defined in Ref. [8]. The hypernuclear polarization  $P_H(J_f)$  of the produced state  $|J_f T_f\rangle$  is defined in  $S_2$  as the sum of the product of  $M_f/J_f$  and the magnetic subspace population  $\mu_{fi}(M_f)$ :

$$P_H(J_f) = \sum_{M_f} \left( \frac{M_f}{J_f} \right) \mu_{fi}(M_f), \quad (5)$$

$$\mu_{fi}(M_f) \equiv R(fi; M_f) / \sum_{M_f} R(fi; M_f).$$

In addition, we also define the  $\Lambda$ -spin polarization in the hypernuclear state  $|J_f T_f\rangle$  as the averaged value of the hyperon Pauli spin. In  $S_2$  it reads

$$P_{\Lambda}(J_f) = \sum_{M_f} \langle J_f M_f | \boldsymbol{\sigma}^{\Lambda} \cdot \hat{\mathbf{n}} | J_f M_f \rangle \mu_{fi}(M_f) \\ = \sqrt{\frac{J_f}{(J_f + 1)(2J_f + 1)}} \langle J_f | | \boldsymbol{\sigma}^{\Lambda} | | J_f \rangle P_H(J_f). \quad (6)$$

The actual calculation of the transition strength  $R(fi; M_f)$  is carried out in the coordinate frame  $S_1$  defined by

$$\{S_1\} \text{ frame : } \hat{\mathbf{z}} = \hat{\mathbf{p}}_a, \quad \hat{\mathbf{y}} = \hat{\mathbf{n}}, \quad \hat{\mathbf{x}} = \hat{\mathbf{y}} \times \hat{\mathbf{z}}, \quad (7)$$

since it is more suitable for evaluation of distorted waves. The coordinate frame  $\{S_2\}$  is obtained from  $\{S_1\}$  by the rotation  $\mathcal{R}(\frac{\pi}{2}, \frac{\pi}{2}, \frac{\pi}{2})$ . Accordingly, the calculated matrix elements in  $S_2$  and  $S_1$  are related by the corresponding

Wigner  $\mathcal{D}$ -function. The  $R(fi; M_f)$  of Eq. (3) is evaluated by means of the partial wave expansion of the product of meson distorted waves in Eq. (1). This quantity can be expressed in terms of the *reduced effective number*  $\rho(fi; M_f)$  as

$$R(fi; M_f) = |f|^2 \rho^{ff}(M_f) + |g|^2 \rho^{gg}(M_f) + 2 \text{Im}[fg^* \rho^{fg}(M_f)] \quad (8)$$

and the meaning of each term is obvious. For example, the value summed over  $M_f$ ,

$$\sum_{M_f} \rho^{ff}(fi; M_f) \equiv N_{\text{eff}}^{ff}(fi),$$

is a generalization (spin-nonflip part) of the usual effective neutron number. The cross section gets contributions dominantly (meson-distortion case) from the former two terms of the right-hand side of Eq. (8),  $|f|^2$  and  $|g|^2$ , while the polarization originates from the  $f$ - $g$  interference term. The detailed expressions for the  $\rho$  matrix in Eq. (8) are given in the appendix in Ref. [8]. Note that, in the case of no meson distortion, the amount of the polarization is proportional to the imaginary part  $\text{Im}[fg^*]$ , as shown in the same reference for particular 1p-1h states such as  $[0p_{\bar{j}}^{-1}0s_{1/2}^{\Lambda}]_J$ .

The hypernuclear polarization  $P_H(J)$  of Eq. (5) and the  $\Lambda$ -spin polarization  $P_{\Lambda}(J)$  of Eq. (6) are nothing but the polarizations on the production stage, respectively. They are of primary importance because they reflect directly the hypernuclear and nuclear (target) structures and the details of reaction mechanism.

In the following we use the elementary amplitude tabulated by Sotona and Žofka [7]. As for the  $\pi^+$  and  $K^+$  distorted waves, we employ the same optical potential parameters as those employed in Ref. [14] so that we can compare the new results with the previous ones. In the partial wave expansions of the meson waves, we confine ourselves to the upper limit  $l_{\text{max}}^{\pi} = l_{\text{max}}^K = 25\hbar$  which is enough for proper convergence at  $r \leq 6$  fm.

## B. Nuclear and hypernuclear wave functions

The Cohen-Kurath model [19] is employed for the target nuclear wave functions, while configuration-mixed shell-model wave functions are solved for the hypernuclear states by adopting the Hamiltonian

$$\mathcal{H} = H_N^{\text{Cohen-Kurath}} + t_{\Lambda} + \xi(\mathbf{1}_{\Lambda} \cdot \mathbf{s}_{\Lambda}) + \sum v_{\Lambda N}. \quad (9)$$

These wave functions are the same as those used in our previous work [14], except for some additional extension of the model space for the  $\Lambda$  hyperon. Thus, in order to show the idea for the final hypernuclear wave functions, we repeat them symbolically as follows:

$$\begin{aligned} \Psi_{\text{I}}(\Lambda Z; JT) &= \sum \alpha_i [(0s)_N^{\Lambda} (0p)_N^{\Lambda-5} \otimes (0s)_{\Lambda}^1]_{JT}, \\ \Psi_{\text{II}}(\Lambda Z; JT) &= \sum \beta_i [(0s)_N^{\Lambda} (0p)_N^{\Lambda-5} \otimes (0p, 1p)_{\Lambda}^1]_{JT}, \\ \Psi_{\text{III}}(\Lambda Z; JT)_k &= [\Phi_N^{\text{core}}(A-1 Z; J_k T_k) \\ &\quad \otimes (1s, 2s, 0d, 1d, 0f, 1f, 0g, 0h)_{\Lambda}^1]_{JT}, \\ \Psi_{\text{IV}}(\Lambda Z; JT) &= [a_{\Lambda}^{\dagger}(nlj) a_N(0s_{1/2}) \Phi_N(\Lambda Z; J_i T_i)]_{JT}, \end{aligned} \quad (10)$$

$$nl = 0s, 0p, 1s, \text{ and } 0d.$$

One should note in the above that the harmonic oscillator  $0p$  and  $1p$  orbits are employed together in  $\Psi_{\text{II}}$  so as to describe the extended radial behavior of the  $p$ -state  $\Lambda$  with shallow binding energy. The wave function of the type  $\Psi_{\text{III}}$  consists of all the eigenstates ( $k = 1, 2, 3, \dots$ ) of nuclear core coupled weakly to the  $\Lambda$  hyperon. The  $\Lambda$  model space is further extended here to simulate the continuum spectrum up to the excitation energy as high as 30–40 MeV. The  $\Lambda$  weak decay from this energy region is observed experimentally. For such high-lying states we use also the wave function  $\Psi_{\text{IV}}$ , which is constructed as the

$$[(0s_{1/2}^N)^{-1}(nlj)_{\Lambda}^{\Lambda}]$$

configuration coupled to the target wave function. Here we have extended the hyperon model space to include  $1s$  and  $0d$  orbits in addition to the one employed in Ref. [14].

We adopted the YNG  $\Lambda N$  effective interaction [20] deduced on the basis of the  $G$ -matrix calculation with Nijmegen model-D force [21]. Here the  $\sigma_{\Lambda} \cdot \sigma_N$  interaction part is modified slightly to meet the requirement for acceptable strength relation between spin-singlet and spin-triplet interactions. As a result, for example, we get the ground-state doublet splitting

$$E(2^-) - E(1_{g.s.}^-) = 160 \text{ keV}$$

for  ${}_{\Lambda}^{10}\text{B}$  and 140 keV for  ${}_{\Lambda}^{12}\text{C}$  ( ${}_{\Lambda}^{12}\text{B}$ ), while

$$E(\frac{7}{2}^+) - E(\frac{5}{2}_{g.s.}^+) = 260 \text{ keV}$$

for  ${}_{\Lambda}^{11}\text{B}$ . In our model the lower spin state is predicted to be the ground state in each case except the  $(p_{1/2}^{-1}s_{1/2}^{\Lambda})$  hypernuclei ( ${}_{\Lambda}^{14}\text{N}$  and  ${}_{\Lambda}^{16}\text{O}$ ). Up to now there are two analyses of pionic decays [22,23] proving the ground-state spins for  ${}_{\Lambda}^{11}\text{B}(\frac{5}{2}^+)$  and  ${}_{\Lambda}^{12}\text{B}(1^-)$ . For the  $p$ -shell hypernuclei with  $A > 10$ , there is no other evidence for the ground-state spin except a  ${}^{10}\text{B}(K^-, \pi^-)_{\Lambda}^{10}\text{B}$  experiment [24] suggesting no  $\gamma$  ray corresponding to the  $2^- \rightarrow 1^-$  transition.

## III. EXCITATION FUNCTION AND CROSS SECTION

In this section the calculated excitation functions and cross section are presented based on the  $f + ig(\boldsymbol{\sigma} \cdot \hat{\mathbf{n}})$  framework, while the polarization will be discussed in the next section. In drawing the smooth excitation functions,

each level is folded with the appropriate Gaussian width  $\Gamma$  depending on its character. Throughout the  $p$ -shell hypernuclei concerned, we adopt the following widths for the levels classified with the expressions of Eq. (10):

$$\Gamma_{\text{FWHM}} = 1.2 \text{ MeV}(\Psi_{\text{I}}), \quad 1.5 \text{ MeV}(\Psi_{\text{II}}), \\ 6.0 \text{ MeV}(\Psi_{\text{III}}), \quad \text{and } 5.0 \text{ MeV}(\Psi_{\text{IV}}).$$

Most of the particle-bound states belonging to  $\Psi_{\text{I}}$  and  $\Psi_{\text{II}}$  should have small physical widths. For these states we use conventional smearing widths (1.2–1.5 MeV), which are comparable to the experimental resolution expected for the INS/KEK superconducting kaon spectrometer (SKS) [25]. For the higher configuration states we use larger widths, which correspond to a typical  $\Lambda$ -escaping width ( $\Psi_{\text{III}}$ ) and the nucleon  $0s$ -hole state width in  $p$ -shell nuclei ( $\Psi_{\text{IV}}$ ) known experimentally. Thus the formation rate of each state is embodied in the combination of the height and the width of a peak.

### A. Excitation function and cross sections for ${}_{\Lambda}^{12}\text{C}$

The upper part of Fig. 1 shows the calculated excitation function of the  ${}^{12}\text{C}(\pi^+, K^+)_{\Lambda}^{12}\text{C}$  reaction at  $p_{\pi} = 1.04 \text{ GeV}/c$  and laboratory scattering angle  $\theta_K = 15^\circ$ . One clearly sees that the ground-state peak of  $J^{\pi} = 1_1^-$  is accompanied with small contribution (about 10%) of the  $2_1^-$  member of the doublet. Note that the latter state is excited only by the spin-flip interaction ( $g$  term) and it is not obtained in the previous treatment [14]. The small bump obtained at  $E_{\Lambda}^{\text{cal}} = -9.01 \text{ MeV}$  (excitation energy  $E_x = 1.75 \text{ MeV}$ ) is due to the  $1_2^-$  state which is characterized by the structure consisting of the first excited state of  ${}^{11}\text{C}(\frac{3}{2}^-)$  and  $s_{1/2}^{\Lambda}$ . Another small peak of  $1_3^-$  is predicted at  $E_{\Lambda}^{\text{cal}} = -5.86 \text{ MeV}$  ( $E_x = 4.90 \text{ MeV}$ ), which is explained by the dominant structure of  $[{}^{11}\text{C}(\frac{3}{2}^-; 4.80 \text{ MeV}) \otimes s_{1/2}^{\Lambda}]$ . Thus we predict three  $1^-$  peaks in the low-energy region as a reasonable consequence of the fact that the Cohen-Kurath model [19] reproduces the lowest six levels in  ${}^{11}\text{C}$  satisfactorily. One should note, on the other hand, that the simplest wave function assuming the  $p_{3/2}$  closure for the  ${}^{12}\text{C}$  target results in only one  $1^-$  state as the ground state. The cross-section ratio for the three peaks is predicted as (cf. Table I)

$$\frac{d\sigma}{d\Omega}(1_1^- + 2_1^-) : \frac{d\sigma}{d\Omega}(1_2^-) : \frac{d\sigma}{d\Omega}(1_3^-) = 1.0 : 0.22 : 0.12$$

$$\text{for } 5^\circ < \theta_K < 15^\circ.$$

Therefore, it is quite interesting to identify such fragmentation of the strength in careful experimental analysis, which then provides a nice confirmation of the hypernuclear wave function.

The strong population of high-spin states is characteristic in the  $(\pi^+, K^+)$  reaction [10,11]. The pronounced peak seen at  $E_{\Lambda} \simeq 0 \text{ MeV}$  ( $E_x \simeq 11 \text{ MeV}$ ) is attributed to the  $2_1^+$  and  $2_2^+$  states calculated at  $E_{\Lambda} = -0.76$  and  $-0.16 \text{ MeV}$  ( $E_x = 10.0$  and  $10.6 \text{ MeV}$ ), respectively. They are both high-spin stretched states having the dominant

structure of

$$[{}^{11}\text{C}(\frac{3}{2}^-; \text{g.s.}) \otimes (p_{3/2}p_{1/2})^{\Lambda}].$$

The substitutional  $0_1^+$  state at  $E_x = 10.8 \text{ MeV}$ , which plays the dominant role in the  $(K^-, \pi^-)$  reaction at  $\theta_{\pi} \sim 0^\circ$ , has a minor contribution to this peak. At higher excitation energies ( $E_x \geq 15 \text{ MeV}$ ), the broad and large bump is seen, composed of many overlapping continuum states. Among them, the high-spin states are populated strongly as a consequence of the selectivity of the reaction.

The momentum transfer  $q$  in the  $(\pi^+, K^+)$  reaction with  $p_{\pi} = 1040 \text{ MeV}/c$  increases gradually as a function of  $\theta_K$ : e.g.,  $q(\theta_K) = 340$  ( $0^\circ$ ),  $349$  ( $5^\circ$ ),  $372$  ( $10^\circ$ ),  $408$  ( $15^\circ$ ),  $453$  ( $20^\circ$ ), and  $500$  ( $25^\circ$ ) in  $\text{MeV}/c$ . It is remarked that  $q(0^\circ)$  is already large enough to favor the high-spin  $p$ -h states and therefore the pattern of relative strengths is not strongly dependent on  $\theta_K$ . This is why we show here the excitation functions for  $\theta_K = 10^\circ$  or  $15^\circ$  together with the polarization.

There exist experimental data [15–18] that show two prominent peaks at the ground state and about 11 MeV

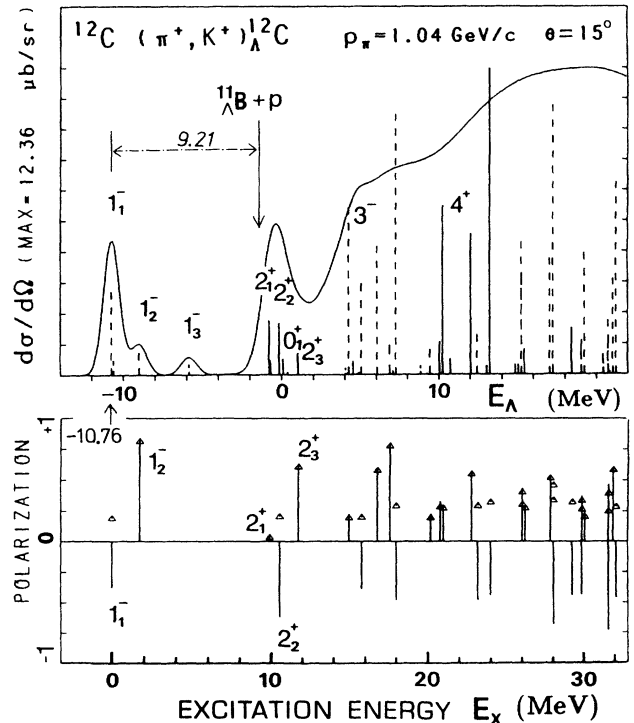


FIG. 1. The excitation function (top) and the polarizations (bottom) calculated for the  ${}^{12}\text{C}(\pi^+, K^+)_{\Lambda}^{12}\text{C}$  reactions at  $p_{\pi+} = 1.04 \text{ GeV}/c$  and at laboratory scattering angle  $\theta_K = 15^\circ$ . In the upper half, the differential cross sections (solid lines for positive parity and dashed lines for negative parity) are represented in relative scale with respect to the maximum value in the concerned energy region which is given in the left parentheses. The smooth excitation function (in units of  $\mu\text{b}/\text{sr MeV}$ ) is drawn also in relative scale by using the smearing widths described at the beginning of Sec. III. In the lower half, the hypernuclear polarization  $P_H(J_n^{\pi})$  is shown by the straight line and the  $\Lambda$ -spin polarization  $P_{\Lambda}(J_n^{\pi})$  by  $\Delta$ .

excitation. Although the 11 MeV peak is affected by the smearing of the continuum background, the calculated energies and cross sections for the two peaks turn out to be in good agreement with the experimental data. (Note that the old ground-state cross section [15] may be underestimated in comparison with the new experiment [17].) In Table I we summarize the calculated cross sections in some detail for the peak states in  ${}_{\Lambda}^{12}\text{C}$ ,  ${}_{\Lambda}^{13}\text{C}$ , and  ${}_{\Lambda}^{16}\text{O}$ . In the table we also list the group cross sections in the square bracket considering the present day energy resolution. In Fig. 2 we display the theoretical and experimental [15] angular distributions for the ground-state and 11 MeV peaks, respectively. In the former peak we sum up the contributions from the  $1_1^-$  and  $1_2^-$  states so as to compare them theoretically with the previous result based on the approximate treatment as

$$\frac{d\sigma}{d\Omega} = \alpha \left( \frac{d\sigma}{d\Omega} \right)_{\text{elem}} N_{\text{eff}}.$$

Actually, the small contribution from  $2_1^-$  should be also added, as in Table I, when one discusses the theory-experiment comparison. For the 11 MeV peak, the summation is taken over the  $0_1^+$ ,  $2_1^+$ , and  $2_2^+$  contributions in the demonstration of Fig. 2 (bottom). However, the minor contribution from the  $3^+$  state at  $E_{\Lambda}^{\text{cal}} = -0.68$  MeV ( $E_x = 10.1$  MeV) should not be neglected, as it is excited only by the spin-flip transition and, in contrast to the normal-parity states, the  $3^+$  state has different angular distribution (cf. Table I). The cross section calculated for the 11 MeV peak is in good agreement with the Brookhaven data [15] observed at  $\theta = 5.6^\circ$ . It is noted in Fig. 2 that the cross sections calculated based on the elementary amplitudes are a little larger than the results of the previous treatment [14].

### B. Excitation function and cross sections for ${}_{\Lambda}^{13}\text{C}$

The calculated excitation function for the  ${}^{13}\text{C}(\pi^+, K^+)_{\Lambda}^{13}\text{C}$  reaction at laboratory scattering angle

TABLE I. Hypernuclear energy levels and differential cross sections calculated for the  $(\pi^+, K^+)$  reactions with  $p_{\pi} = 1.04$  GeV/c and laboratory scattering angles  $\theta_K = 5^\circ, 10^\circ, \text{ and } 15^\circ$ . In the square brackets are shown the summed cross sections over the nearly degenerate states not to be separated within the assumed experimental resolution.

	Level energy $E_{\Lambda}$ (MeV)		$d\sigma/d\Omega$ ( $\mu\text{b/sr}$ )			EXP ( $\theta_K$ )	
	EXP <sup>a</sup>	CAL ( $J^{\pi}; E_x$ )	CAL ( $5^\circ$ )	CAL ( $10^\circ$ )	CAL ( $15^\circ$ )		
${}_{\Lambda}^{12}\text{C}$	-10.75	-10.76 <sup>b</sup> ( $1_1^-$ ; g.s.) <sup>*</sup>	12.48 [15.4 <sup>c</sup> ]	7.73[10.3 <sup>c</sup> ]	3.36[4.9 <sup>c</sup> ]	[8.5(10.3 <sup>o</sup> ) <sup>e</sup> ] and [10.36 $\pm$ 0.61(10 <sup>o</sup> ) <sup>f</sup> ]	
		-10.52( $2_1^-$ ;0.14) <sup>*</sup>	0.28	0.67	0.62		
		-9.01( $1_2^-$ ;1.75) <sup>*</sup>	2.65	1.84	0.91		
		-5.86( $1_3^-$ ;4.90)	1.60	1.00	0.44		
		-0.76( $2_1^+$ ;10.0) <sup>**</sup>	9.08	5.52	2.19		
		-0.68( $3_1^+$ ;10.1) <sup>**</sup>	0.29	0.69	0.60		
	-0.5	-0.16( $2_2^+$ ;10.6) <sup>**</sup>	7.08 [17.6 <sup>d</sup> ]	4.58 [12.8 <sup>e</sup> ]	2.09 [5.5 <sup>d</sup> ]	[17.0(5.6 <sup>o</sup> ) <sup>e</sup> ]	
		0.10( $0_1^+$ ;10.9) <sup>**</sup>	1.10	1.03	0.65		
		1.02( $2_3^+$ ;11.8)	3.08	2.03	0.88		
	${}_{\Lambda}^{13}\text{C}$	-11.5	-11.69 <sup>b</sup> ( $\frac{1}{2}_1^+$ ; g.s.)	2.97	1.99	0.91	
-6		-7.05( $\frac{3}{2}_1^+$ ;4.60)	4.59	2.79	1.16		
-2		-1.69( $\frac{3}{2}_1^-$ ;10.0)	3.79	2.51	1.06		
		-1.13( $\frac{1}{2}_1^-$ ;10.6)	0.15	0.20	0.16		
		0.52( $\frac{1}{2}_2^+$ ;12.2)	3.20	1.93	0.79		
		3.31( $\frac{5}{2}_1^+$ ;15.0)	8.04	6.93	4.70		
4		3.34( $\frac{5}{2}_1^-$ ;15.0)	4.08	2.57	1.11		
		4.82( $\frac{3}{2}_2^+$ ;16.5)	3.54	2.15	0.90		
${}_{\Lambda}^{16}\text{O}$		-12.50	-13.0 <sup>b</sup> ( $1_1^-$ ; g.s.)	6.14	3.81	1.64	1.68 $\pm$ 0.36(10 <sup>o</sup> ) <sup>f</sup>
		-6	-6.81( $1_2^-$ ;6.23)	9.80	5.63	2.24	
	-2.5	-2.74( $2_1^+$ ;10.3)	8.34	5.13	2.04		
		-1.80( $0_1^+$ ;11.2)	0.39	0.34	0.20		
		3.54( $2_2^+$ ;16.6) <sup>†</sup>	8.39	4.80	1.79		
	4.5	4.16( $2_3^+$ ;17.2) <sup>†</sup>	7.57 [17.6 <sup>g</sup> ]	4.60 [10.4 <sup>g</sup> ]	1.93 [4.3 <sup>g</sup> ]		
		4.38( $0_2^+$ ;17.4) <sup>†</sup>	1.16	1.01	0.58		

<sup>a</sup>The  $\Lambda$  energies for the peaks are taken from the figures in Refs. [16,17].

<sup>b</sup>The calculated energies are shown with respect to the ground-state  $\Lambda$  energy  $E_{\Lambda}(\text{g.s.})$  taken from the emulsion data for  ${}_{\Lambda}^{12}\text{C}$  and  ${}_{\Lambda}^{13}\text{C}$  and from the density-dependent Hartree-Fock (DDHF) calculation [12] for  ${}_{\Lambda}^{16}\text{O}$ .

<sup>c</sup> $1_1^- + 2_1^- + 1_2^-$  (sum of the states with the asterisk).

<sup>d</sup> $2_1^+ + 3_1^+ + 2_2^+ + 0_1^+$  (sum of the states with the double asterisk).

<sup>e</sup>Reference [15].

<sup>f</sup>Reference [17].

<sup>g</sup> $2_2^+ + 2_3^+ + 0_2^+$  (sum of the states with the double dagger).

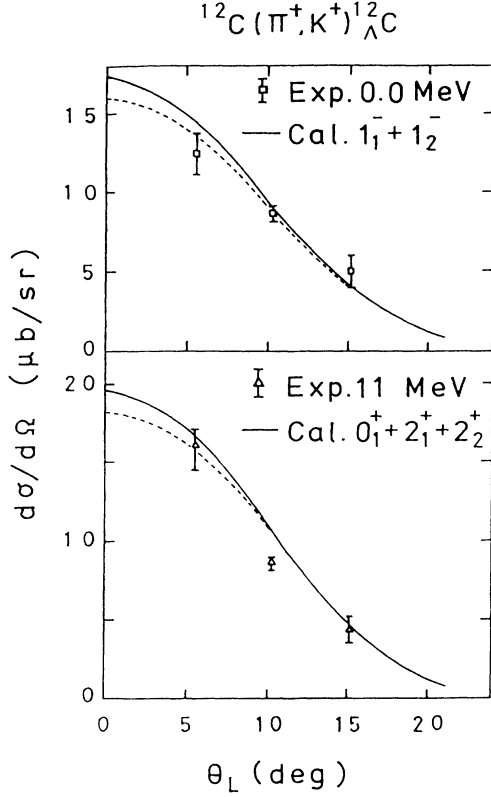


FIG. 2. The angular distribution of the cross sections for the ground-state and 11-MeV peaks in  $^{12}\text{C}$ . The present calculation with the elementary amplitudes (solid) and the previous approximation (dashed) [14] of  $d\sigma/d\Omega = \alpha(d\sigma/d\Omega)_{\text{elem}} N_{\text{eff}}$  are compared with the experimental data [15].

$\theta_K = 10^\circ$  is displayed in Fig. 3 (top), where three distinct peaks are clearly recognized in the bound-state region below the  $^{12}\text{C} + \Lambda$  threshold at  $E_x = 11.69$  MeV. Their spins are  $\frac{1}{2}_1^+$  (g.s.),  $\frac{3}{2}_1^+$  ( $E_\Lambda^{\text{cal}} = -7.05$ ;  $E_x = 4.60$  MeV) and  $\frac{3}{2}_1^-$  ( $E_\Lambda^{\text{cal}} = -1.69$ ;  $E_x = 10.0$  MeV). The former two states are naturally characterized by the dominant structures of

$$[^{12}\text{C}(0^+; \text{g.s.}) \otimes s_{1/2}^\Lambda]_{1/2^+}$$

and

$$[^{12}\text{C}(2_1^+; E_x = 4.40 \text{ MeV}) \otimes s_{1/2}^\Lambda]_{3/2^+},$$

respectively, as revealed from the wave function analysis [14]. The third peak has the structure

$$[^{12}\text{C}(0_{\text{g.s.}}^+) \otimes p_{3/2}^\Lambda]_{3/2^-}.$$

Thus we have a possibility of observing  $\gamma$  rays from these excited states, which provide high-resolution information on the level energies (especially the  $s_{1/2}$ - $p_{3/2}$  splitting from the  $\frac{3}{2}_1^- \rightarrow \frac{1}{2}_{\text{g.s.}}^+$  transition). The  $\frac{3}{2}_1^-$  state is strongly excited by the  $L = 2$  transition, which dominates in the  $(\pi^+, K^+)$  reaction.

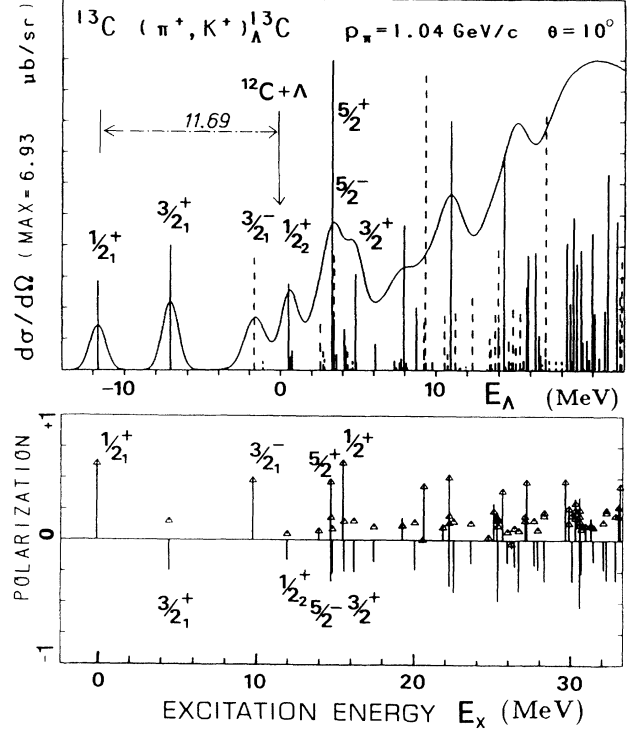


FIG. 3. The excitation function (top) and the polarizations (bottom) calculated for the  $^{13}\text{C}(\pi^+, K^+)_{\Lambda}^{13}\text{C}$  reactions at  $p_{\pi^+} = 1.04$  GeV/c and  $\theta_K = 10^\circ$ . See also the caption of Fig. 1.

It should be noted here that the spin-orbit partner state with  $p_{1/2}^\Lambda$  ( $J = \frac{1}{2}^-$ ) is not so strongly excited as the  $\frac{3}{2}_1^-$  state. The reason is because the  $\frac{1}{2}^-$  state is excited only through the  $L = 0$  transition and hence the small matrix element of

$$|\langle 0p^\Lambda | \tilde{j}_{L=0}(\theta; r) | 0p^N \rangle|^2$$

is involved. (Also the kinematical factor  $2j + 1$  unfavors the  $\frac{1}{2}^-$  state.) This means that the situation becomes opposite in the forward  $(K^-, \pi^- \gamma)$  reaction and that the comparison between  $(\pi^+, K^+ \gamma)$  and  $(K^-, \pi^- \gamma)$  experiments is necessary to extract the  $\Lambda$  spin-orbit splitting.

In the calculation we also predict fourth and fifth peaks just above the  $\Lambda$ -escaping threshold. The fourth one is calculated at  $E_\Lambda^{\text{cal}} = 0.52$  MeV ( $E_x = 12.2$  MeV) to have the dominant structure of

$$[^{12}\text{C}(1^+) \otimes s_{1/2}^\Lambda]_{1/2^+}.$$

The bigger and fifth one consists of several resonances including the dominant structures of

$$[^{12}\text{C}(2_1^+) \otimes p_{1/2}^\Lambda]_{5/2^-}$$

and

$$[^{12}\text{C}(0_1^+) \otimes d_{5/2}^\Lambda]_{5/2^+}.$$

The excitation function in Fig. 3 is in reasonable agree-

ment with the Brookhaven data [15,16] taken at  $\theta_K = 10^\circ$ . The estimates of the relevant cross sections are listed in Table I at three different scattering angles. It is reasonable that the ground-state cross section is calculated to be about four times smaller than the corresponding strength in  $^{12}\text{C}$ , since a  $p_{1/2}$  neutron is converted to populate the low-lying states in  $^{13}\text{C}$ .

### C. Excitation function and cross sections for $^{16}\text{O}$

The calculated spectrum for the  $^{16}\text{O}(\pi^+, K^+)_{\Lambda}^{16}\text{O}$  reaction at  $p_\pi = 1.04 \text{ GeV}/c$  and  $\theta_K = 10^\circ$  is displayed in Fig. 4 where we obtain four distinct peaks in very good agreement with the experiment [16]. It is well known [26,27] that the  $1_1^-$  and  $2_1^+$  peaks obtained here at  $E_\Lambda^{\text{cal}} = -13.04 \text{ MeV}$  (g.s.) and  $-2.74 \text{ MeV}$  ( $E_x = 10.30 \text{ MeV}$ ) are based on the  $p_{1/2}$  neutron hole state, i.e.,  $\frac{1}{2}^-$  in  $^{15}\text{O}$ . Thus they are attributed to the  $(p_{1/2}^- s_{1/2}^\Lambda)_{1-}$  and  $(p_{1/2}^- p_{3/2}^\Lambda)_{2+}$  structures, respectively. Furthermore, the second and fourth peaks are originated from the  $p_{3/2}$  neutron state in  $^{15}\text{O}$ . The former peak obtained at  $E_\Lambda^{\text{cal}} = -6.81 \text{ MeV}$  ( $E_x = 6.23 \text{ MeV}$ ) is due to the  $(p_{3/2}^- s_{1/2}^\Lambda)_{1-}$  structure and the latter peak at  $E_\Lambda^{\text{cal}} \simeq 4 \text{ MeV}$  ( $E_x \simeq 17 \text{ MeV}$ ) consists of two  $2^+$  states of the  $[p_{3/2}^- (p_{3/2} p_{1/2})^\Lambda]$  configuration. This peak appears to be a considerably narrow resonance on the broad background of continuum contribution from the  $[p_{1/2}^- (1s0d)^\Lambda]_{3-,1-}$  states. As the

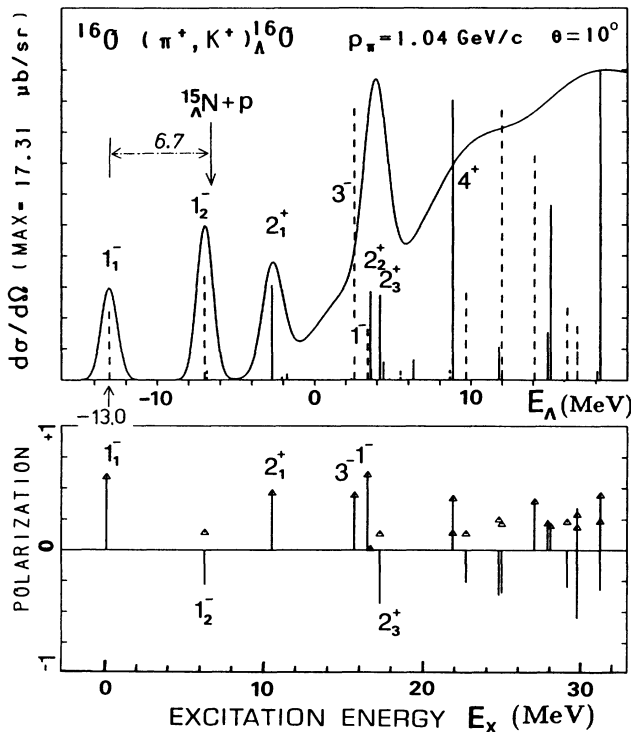


FIG. 4. The excitation function (top) and the polarizations (bottom) calculated for the  $^{16}\text{O}(\pi^+, K^+)_{\Lambda}^{16}\text{O}$  reactions at  $p_{\pi^+} = 1.04 \text{ GeV}/c$  and  $\theta_K = 10^\circ$ . See also the caption of Fig. 1.

experimental energy splitting between  $p_{1/2}^-$  and  $p_{3/2}^-$  in  $^{15}\text{O}$  is 6.18 MeV, the peak energies in  $^{16}\text{O}$  provide the  $\Lambda$ -shell splitting  $\Delta E(p-s) \simeq 10 \text{ MeV}$ . It should be pointed out that, if the energy resolution is good enough, the comparison between the  $(K^-, \pi^-)$  and  $(\pi^+, K^+)$  spectra provides us the details of  $\Lambda N$  interaction through the spectroscopic analysis of the  $[p_{1/2}^- p^\Lambda]_{0+,2+}$  multiplet splittings. We note here that the  $0^+$  state appears at higher energy than two  $2^+$  states due to the more repulsive nature of the  $\Lambda$ -h interaction.

### D. Excitation functions and cross sections predicted for $^{10}\text{B}$ , $^{11}\text{B}$ , and $^{14}\text{N}$

The excitation functions for other available  $p$ -shell targets ( $^{10}\text{B}$ ,  $^{11}\text{B}$ , and  $^{14}\text{N}$ ) are calculated for the  $(\pi^+, K^+)_{\Lambda}$  reactions at  $p_\pi = 1.04 \text{ GeV}/c$  and  $\theta_K = 10^\circ$ , although we have no experimental data up to now. The results are shown in the upper half of Figs. 5, 6, and 7, respectively.

In Fig. 5 (top) we obtain four high-spin pronounced peaks in the  $^{10}\text{B}$  spectrum below  $E_x \simeq 10 \text{ MeV}$ . Each energy separation is predicted to be about 3 MeV or more, which should be suitable for the experimental identification. This feature has been already pointed out in the previous paper [14] as a characteristic merit of the  $(\pi^+, K^+)_{\Lambda}$  reaction providing large  $L = 1$  transition. Thus the  $(\pi^+, K^+)_{\Lambda}$  experiment will yield a useful restriction on the feature of  $\Lambda$  coupling to the four nuclear core states

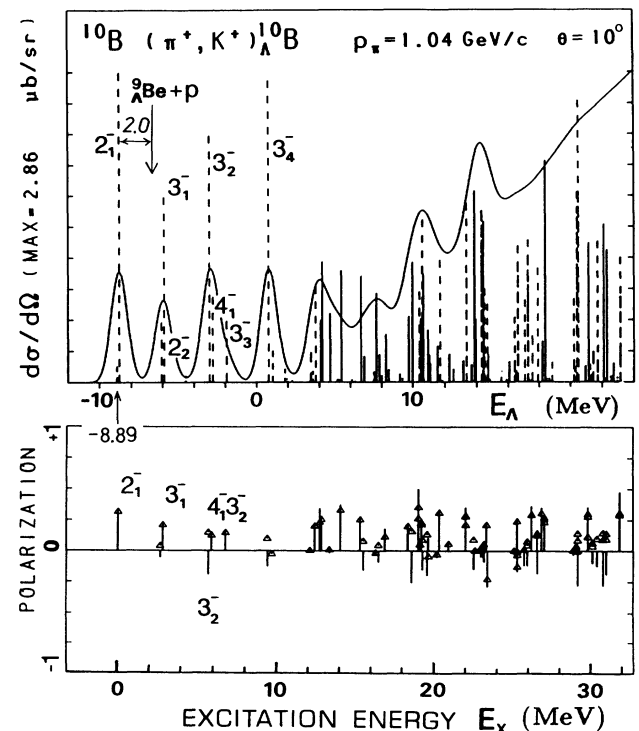


FIG. 5. The excitation function (top) and the polarizations (bottom) calculated for the  $^{10}\text{B}(\pi^+, K^+)_{\Lambda}^{10}\text{B}$  reactions at  $p_{\pi^+} = 1.04 \text{ GeV}/c$  and  $\theta_K = 10^\circ$ . See also the caption of Fig. 1.

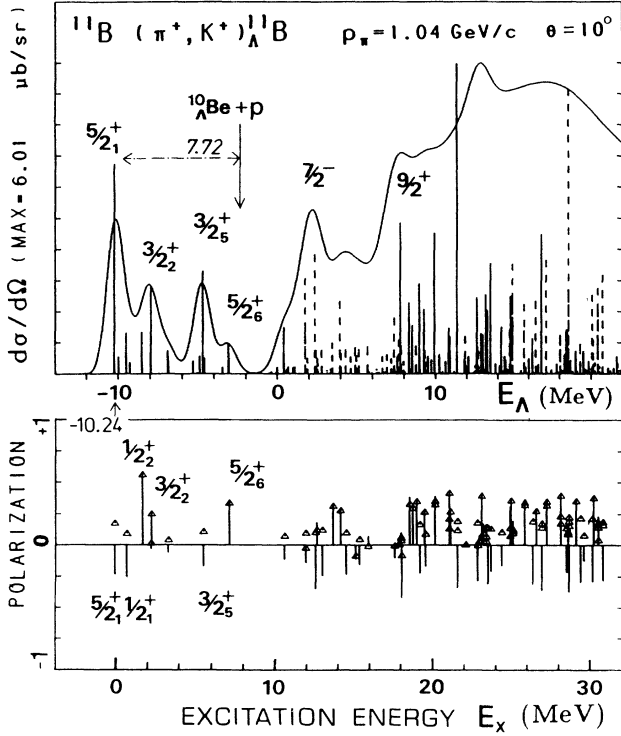


FIG. 6. The excitation function (top) and the polarizations (bottom) calculated for the  $^{11}\text{B}(\pi^+, K^+)_{\Lambda}^{11}\text{B}$  reactions at  $p_{\pi^+} = 1.04 \text{ GeV}/c$  and at  $\theta_K = 10^\circ$ . See also the caption of Fig. 1.

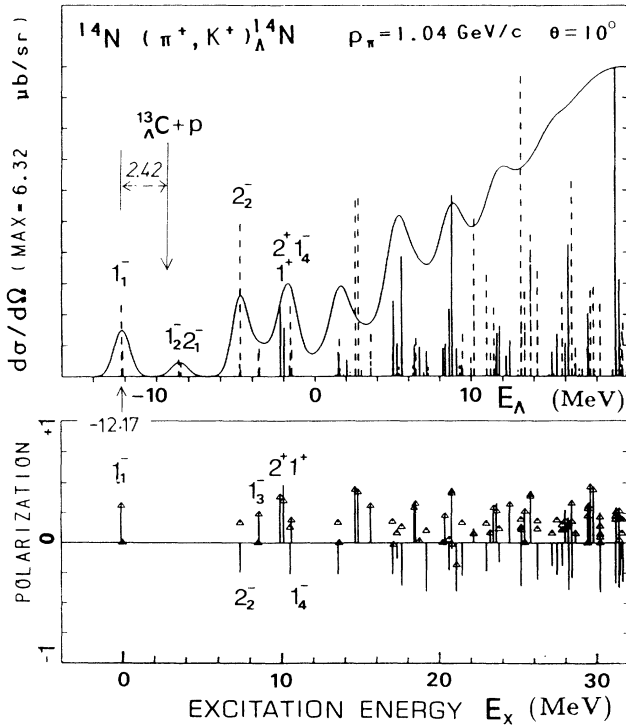


FIG. 7. The excitation function (top) and the polarizations (bottom) calculated for the  $^{14}\text{N}(\pi^+, K^+)_{\Lambda}^{14}\text{N}$  reactions at  $p_{\pi^+} = 1.04 \text{ GeV}/c$  and  $\theta_K = 10^\circ$ . See also the caption of Fig. 1.

in  $^9\text{Be}$ . It is remarked that we hardly expect to see these low-lying states in the forward ( $K^-, \pi^-$ ) reaction because the  $L = 1$  transition rate from the target of  $^{10}\text{B}(3^+)$  is very small at  $\theta_{\pi} \simeq 0^\circ$  in comparison with the substitutional  $L = 0$  transition.

The  $2^-, 3_1^-, 3_2^-,$  and  $3_4^-$  states are composed of the  $s_{1/2}$   $\Lambda$  particle coupled to the  $\frac{3}{2}^-$  (g.s.),  $\frac{5}{2}^-$  ( $E_x = 2.36 \text{ MeV}$ ),  $\frac{7}{2}^-$  (6.97 MeV), and  $\frac{7}{2}^-$  (11.70 MeV) states in  $^9\text{B}$ , respectively. These nuclear core states are well reproduced in the Cohen-Kurath model [19] so far as their energies are concerned.

The structure of the target  $^{10}\text{B}(J = 3^+)$  can be described by  $[p_{3/2}^6(v = 2; T = 0)]_{3+}$  in the  $j-j$  coupling or

$$[\pi p^3(1^-) \nu p^3(1^-) L = 2, S = 1]_{3+}$$

in the  $L-S$  coupling to a good approximation. Therefore, the  $2^-$  member ( $L = 1, S = 1$ ) of the ground doublet is preferentially excited by the spin-nonflip transition of  $L = 1$  ( $p_{3/2}^N \rightarrow s_{1/2}^{\Lambda}$ ), while the  $1^-$  member is only weakly populated by the minor spin-flip transition. The spin structures of the higher-energy levels are not so pure, but it is notable that the unnatural parity states such as  $2^-$  in the second peak and  $4^-$  in the third peak are excited weakly in the present calculation. Three peaks higher than the ground state decay to  $^9\text{Be}$  by emitting a proton, so that the  $(\pi^+, K^+)$  reaction on  $^{10}\text{B}$  provides the adjacent hypernucleus. The predicted yields for the remarked peaks are appreciable ( $2-3 \mu\text{b}/\text{sr}$  at  $\theta_K = 10^\circ$ ).

The  $(\pi^+, K^+)$  reaction on the target  $^{11}\text{B}(\frac{3}{2}^-)$  leads to many low-lying states below the  $^{10}\text{B}+p$  threshold in  $^{11}\text{B}$ . In the bound-state region, which is hardly accessed in the forward ( $K^-, \pi^-$ ) reaction [14], we get the ground-state large peak of  $\frac{5}{2}^+$  only through the  $(\pi^+, K^+)$  process. Furthermore, one may add two peaks with appreciable strength:  $\frac{3}{2}^+$  ( $E_{\Lambda}^{\text{cal}} = -7.95 \text{ MeV}$ ;  $E_x = 2.29 \text{ MeV}$ ) and  $\frac{3}{2}^+$  ( $T = 1, E_{\Lambda}^{\text{cal}} = -4.70 \text{ MeV}$ ;  $E_x = 5.54 \text{ MeV}$ ). However, the dense energy levels in the  $^{11}\text{B}$  bound-state region, which reflect the high level density of  $^{10}\text{B}$ , do not favor the spectroscopic approach to the hypernuclear structure without high-resolution detectors. Nevertheless, all the production strengths of the bound states are summed up to feed the ground state, which should be used for the study of its weak decay.

Experimentally, only the  $(K^-, \pi^-)$  reaction at  $p_K = 800 \text{ MeV}/c$  and  $\theta_{\pi} = 0^\circ$  has been attempted to produce the  $^{14}\text{N}$  hypernucleus, disclosing two substitutional big peaks at  $E_x = 10$  and  $19 \text{ MeV}$  in addition to the small ground-state peak [28]. Here we are concerned with the  $(\pi^+, K^+)$  reaction on  $^{14}\text{N}(1_{\text{g.s.}}^+)$ , which can easily populate the low-lying states due to the sizable momentum transfer. We predict four distinguishable peaks in the  $\Lambda$  bound-state region ( $E_{\Lambda} < 0 \text{ MeV}$ ), as shown in Fig. 7 (top). The lowest three peaks obtained at  $E_x = 0.0, 3.59,$  and  $7.48 \text{ MeV}$  have the simplest weak-coupling structures,

$$[^{13}\text{N}(\frac{1}{2}^-; \text{g.s.}) \otimes s_{1/2}^{\Lambda}]_{1-},$$

$$[^{13}\text{N}(\frac{3}{2}^-; 3.5 \text{ MeV}) \otimes s_{1/2}^{\Lambda}]_{1-, 2-},$$

$$[^{13}\text{N}(\frac{5}{2}^-; 7.4 \text{ MeV}) \otimes s_{1/2}^{\Lambda}]_{2-},$$

respectively. The fourth peak consists of several states with both positive and negative parities. Note that only the ground  $1^-$  state is particle stable and the other states lead to the daughter hypernucleus  ${}^{13}_{\Lambda}\text{C}$  by emitting a proton.

Here we give a comment on the comparison between the new excitation functions and the previous results [14]. The old prescription of

$$\frac{d\sigma}{d\Omega} = \alpha \left( \frac{d\sigma}{d\Omega} \right)_{\pi n \rightarrow \Lambda K}^{\text{EXP}} N_{\text{eff}}$$

corresponds to the approximation that, instead of Eqs. (4) and (8), only the spin-nonflip part ( $f$ ) is taken into account with necessary renormalization. The present calculation reveals that the basic character of the excitation functions is the same in both calculations and also that the magnitudes of the cross sections are more or less similar. This is because the spin-nonflip and spin-flip terms contribute additively to the cross section, and the former term is still dominant in the  $(\pi^+, K^+)$  reaction at small scattering angles (cf. Fig. 8) in the energy region under discussion. In the present calculation, of course, there appear the essentially new states excited only by the spin-flip interaction.

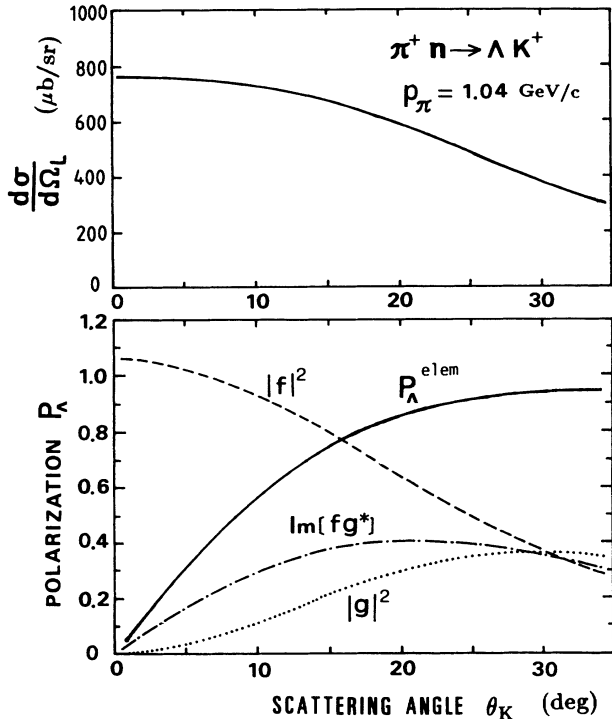


FIG. 8. The spin-nonflip amplitude ( $f$ ), spin-flip one ( $g$ ), differential cross section, and polarization calculated as a function of the laboratory scattering angle for  $\pi^+ n \rightarrow \Lambda K^+$  at  $p_\pi = 1.04$  GeV/c. See Eq. (1) for the definition of the amplitudes and Eq. (11) for the  $\Lambda$  polarization in the free space. The two-body laboratory cross section is given by  $d\sigma/d\Omega = C(|f|^2 + |g|^2)$  where  $C$  is a proportionality coefficient [7].

#### IV. POLARIZATIONS PRODUCED IN THE REACTION

The hypernuclear polarization comes from two origins. One is the meson-wave distortion (near-side vs far-side mechanism), which effect is known to be small up to laboratory scattering angle  $\theta \simeq 15^\circ$  and then it increases gradually with a negative sign [5,8]. The other is the main source of polarization and is due to the strong spin-flip interaction ( $g$  term) in the elementary  $\pi^+ n \rightarrow \Lambda K^+$  process. By choosing particular scattering angles, Ref. [8] has demonstrated the incident-pion momentum dependence of the cross section and the polarization in the elementary process ( $1.0 < p_\pi < 2.4$  GeV/c).

For the following discussions, here in Fig. 8 we show the scattering angle dependence of the elementary amplitudes, cross section, and polarization at the fixed pion momentum,  $p_\pi = 1.04$  GeV/c. One sees that the polarization (spin polarization in this case) increases remarkably as a function of  $\theta_K$  to exceed 75% at  $\theta_K > 15^\circ$ . The spin-nonflip amplitude ( $f$ ) is dominant and decreases as  $\theta_K$ , while the minor spin-flip amplitude ( $g$ ) increases from 0 to the value comparable to  $f$ . The latter behavior, through the  $f$ - $g$  interference, is responsible for the  $\Lambda$  polarization, since it is given by

$$P_\Lambda^{\text{elem}} = \frac{2 \text{Im}(fg^*)}{|f|^2 + |g|^2}. \quad (11)$$

The elementary cross section decreases gradually from 800  $\mu\text{b/sr}$  to 300  $\mu\text{b/sr}$  for  $0^\circ < \theta_K < 35^\circ$  as shown in Fig. 8 (top). It should be noted, however, that the hypernuclear production cross section decreases much faster with increasing  $\theta_K$ . Then there is an optimum scattering angle where the quantity  $P^2(d\sigma/d\Omega)$  becomes maximum for experimental feasibility. This is why we presented the excitation functions at  $\theta_K = 10^\circ$ – $15^\circ$  in Sec. III.

Two origins mentioned above are both taken into account to get hypernuclear and  $\Lambda$ -spin polarizations. Here we are interested mostly in such states that have considerable production rates and sizable polarizations at the same time. Thus, in every figure, we show the polarization in the lower half in combination with the excitation function in the upper half. The hypernuclear polarization  $P_H$  of Eq. (5) is indicated in each lower half by a straight line and the  $\Lambda$ -spin polarization  $P_\Lambda$  of Eq. (6) is indicated by an open triangle.

##### A. Polarizations in the ${}^{12}_{\Lambda}\text{C}$ production

The calculated results in the  $(\pi^+, K^+)$  production of the  ${}^{12}_{\Lambda}\text{C}$  states are shown in the lower half of Fig. 1. First, if we look at the states below the  $\Lambda$ -escape threshold ( $E_\Lambda < 0$  or  $E_x < 10.76$  MeV), we get three states that have large hypernuclear polarization. Their magnitudes predicted at  $\theta_K = 15^\circ$  are

$$P_H(1_1^-) = -0.38, \quad P_H(1_2^-) = 0.81,$$

and

$$P_H(2_2^+) = -0.62,$$

respectively. See Table II for the values at  $\theta_K = 5^\circ$  and  $10^\circ$ . It is notable that the  $2_1^+$  state obtained at  $E_x = 10.0$  MeV has a very small polarization,  $P_H(2_1^+) = 0.04$ , although it has sizable production strength comparable to that of the  $2_2^+$  state.

First, it is interesting to compare the present estimates with the previous ones [8] which were calculated by using the simplest 1p-1h wave function. The use of the mixed wave functions for  ${}^{12}_\Lambda\text{C}$  reduces the ground-state polarization  $P_H(1_1^-)$  by 20% with respect to the estimate based on the  $(p_{3/2}^{-1}s_{1/2}^\Lambda)_{1-}$  assumption (cf. Table II). On the other hand, the present calculation enlarges  $P_H(2_2^+)$  in comparison with the  $(p_{3/2}^{-1}p_{1/2}^\Lambda)_{2+}$  estimate.

Second, for typical states, the angular dependence of the hypernuclear polarization is shown in Fig. 9, where the comparison is also made with the single-configuration estimates of  $(p_{3/2}^{-1}j^\Lambda)$ . The magnitudes of the polarization increase with the laboratory angle  $\theta_K$  except for  $2_1^+$ . This is mainly due to the increase of the  $g$  amplitude (cf. Fig. 8),  $g = g_1(s, t) \sin \theta$ , where  $s$  and  $t$  are invariants and the c.m. scattering angle  $\theta$  has a well-known relation to the laboratory angle. Large polarizations are obtained at  $\theta_K \geq 10^\circ$ . It is noted, however, that the cross section decreases at large angles in general (see Fig. 2). Therefore, the optimal angle for the coincidence experiment such as the asymmetry measurement of the weak-decay particle should be chosen to maximize  $P^2(d\sigma/d\Omega)$ . (In the present case we get  $\theta_K \simeq 14^\circ$ .)

Also in Fig. 9 the polarizations of  $1_1^-$  and  $2_2^+$  calculated in DWIA are compared with those of PWIA (dotted). The difference is due to the meson-wave-distortion contribution to the polarization and its effect is shown to be small at least up to the angles  $\theta_K \sim 20^\circ$ . Thus we know that the large polarizations for  $1_1^-$  and  $2_2^+$ , and also for  $1_2^-$ , originate from the elementary  $\Lambda$ -spin polarization. In this connection, it is noted that the polarization of  $2_1^+$  originates from the distortion-oriented polarization.

Third, we remark that the signs of polarizations are different between the ground and the first excited states ( $1_1^-$  vs  $1_2^-$ ). The reason is as follows. As is known from the structures of the target and the hypernucleus, the  $1_1^-$  state is excited exclusively through the  $p_{3/2}^N \rightarrow s_{1/2}^\Lambda$  transition, while the  $1_2^-$  state is excited through the  $p_{1/2}^N \rightarrow s_{1/2}^\Lambda$  transition. Polarization is mainly induced by the interference between the spin-nonflip ( $f$ ) and the spin-flip ( $g$ ) terms in the transition interaction. Thus  $P_H(1_1^-)$  and  $P_H(1_2^-)$  are determined by the following product of the single-particle transition matrix elements in the  $S_1$  frame:

$$\langle s_{1/2}^\Lambda || \tilde{j}_{1M_1} Y_1 || p_j^N \rangle \langle s_{1/2}^\Lambda || \tilde{j}_{1M_2} [Y_1 \times \sigma]_{K=1} || p_j^N \rangle^*,$$

$$j = \frac{3}{2} \text{ or } \frac{1}{2}. \quad (12)$$

Here  $\tilde{j}_{LM}(r; p_\pi, p_K, \theta)$  is the  $L$ th partial wave in the expansion of the product of meson distorted waves. It

TABLE II. Hypernuclear polarizations ( $P_H$ ) and  $\Lambda$ -spin polarizations ( $P_\Lambda$ ) calculated for the  $(\pi^+, K^+)$  reactions with  $p_\pi = 1.04$  GeV/c leading to the typical states in  ${}^{12}_\Lambda\text{C}$ ,  ${}^{13}_\Lambda\text{C}$ , and  ${}^{16}_\Lambda\text{O}$ . QF denotes the  $\Lambda$ -spin polarization ( $\bar{P}_\Lambda$ ) in the quasifree region averaged over the indicated energies. In the last line the  $\Lambda$  polarization of the elementary process is listed for reference.

	$E_\Lambda^{\text{cal}}(J^\pi; E_x)$ (MeV)	Polarization $P_H$ [ $P_\Lambda$ ]		
		$\theta_K = 5^\circ$	$\theta_K = 10^\circ$	$\theta_K = 15^\circ$
${}^{12}_\Lambda\text{C}$	$-10.76^{\text{a}}(1_1^-; \text{g.s.})$	$-0.12$ [0.06]	$-0.25$ [0.12]	$-0.38$ [0.19]
	$-9.01(1_2^-; 1.75)$	$0.38$ [0.38]	$0.65$ [0.65]	$0.81$ [0.81]
	$-0.76(2_1^+; 10.00)$	$0.04$ [0.02]	$0.07$ [0.04]	$0.05$ [0.03]
	$-0.16(2_2^+; 10.61)$	$-0.24$ [0.08]	$-0.45$ [0.14]	$-0.62$ [0.21]
	$1.02(2_3^+; 11.78)$	$0.27$ [0.27]	$0.48$ [0.48]	$0.60$ [0.60]
	QF ( $15 \leq E_x < 35$ )	[0.14]	[0.25]	[0.33]
	Ref. [8] $(p_{3/2}^{-1}s_{1/2}^\Lambda)_{1g,\text{s.}}$	$-0.16$ [0.08]	$-0.33$ [0.16]	$-0.50$ [0.25]
Ref. [8] $(p_{3/2}^{-1}p_{3/2}^\Lambda)_{2_1^+}$	$0.010$ [0.006]	$0.003$ [0.002]	$-0.033$ [-0.022]	
Ref. [8] $(p_{3/2}^{-1}p_{1/2}^\Lambda)_{2_2^+}$	$-0.23$ [0.08]	$-0.44$ [0.15]	$-0.61$ [0.20]	
${}^{13}_\Lambda\text{C}$	$-11.69^{\text{a}}(\frac{1}{2}_1^+; \text{g.s.})$	$0.35$ [0.35]	$0.61$ [0.61]	$0.77$ [0.77]
	$-7.05(\frac{3}{2}_1^+; 4.60)$	$-0.12$ [0.07]	$-0.25$ [0.15]	$-0.38$ [0.23]
	$-1.69(\frac{3}{2}_1^-; 10.00)$	$0.28$ [0.28]	$0.48$ [0.48]	$0.59$ [0.59]
	QF ( $15 \leq E_x < 35$ )	[0.12]	[0.22]	[0.31]
${}^{16}_\Lambda\text{O}$	$-13.0^{\text{b}}(1_1^-; \text{g.s.})$	$0.34$ [0.34]	$0.59$ [0.59]	$0.75$ [0.75]
	$-6.81(1_2^-; 6.23)$	$-0.14$ [0.07]	$-0.28$ [0.14]	$-0.43$ [0.21]
	$-2.74(2_1^+; 10.30)$	$0.26$ [0.26]	$0.46$ [0.46]	$0.58$ [0.58]
	QF ( $15 \leq E_x < 35$ )	[0.14]	[0.26]	[0.37]
Elementary process: $\pi^+ n \rightarrow \Lambda K^+$		[0.32]	[0.57]	[0.75]

<sup>a</sup>The calculated energies are shown with respect to the experimental ground-state  $\Lambda$  energy taken from the emulsion data.

<sup>b</sup>Reference [12].

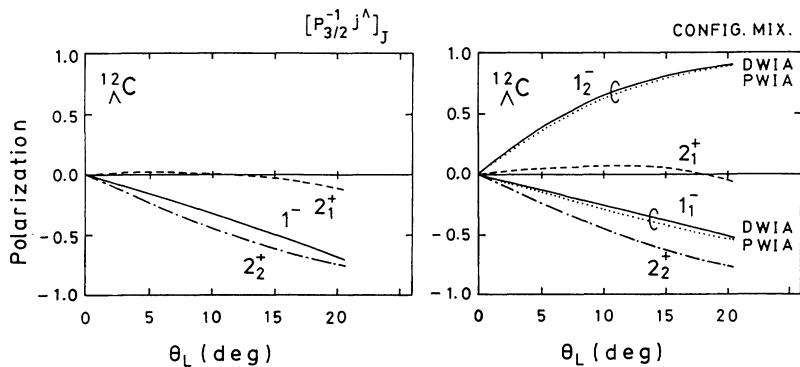


FIG. 9. The angular dependence of the hypernuclear polarization  $P_H(J)$  of  ${}^{12}_{\Lambda}\text{C}$  ( $J = 1_1^-, 1_2^-, 2_1^+$ , and  $2_2^+$ ) as calculated in DWIA with the mixed wave functions (right). For comparison, the PWIA results (dotted line) are also shown for the  $1_1^-$  and  $2_2^+$  states. The left half shows the results of the simple configuration.

is noted that, because of the opposite spin directions between  $p_{3/2}^N$  and  $p_{1/2}^N$ , the sign of Eq. (12) for the dominant component of  $1_1^-$  is different from that of  $1_2^-$ , and hence  $P_H(1_1^-) < 0 < P_H(1_2^-)$ .

As far as the magnitudes of  $P_H(1_1^-)$  and  $P_H(1_2^-)$  are concerned, they depend mostly on the relative strength between the spin-nonflip ( $f$ ) and spin-flip ( $g$ ) single-particle matrix elements in Eq. (12). Note that the radial integral parts are practically the same for both states. For the  $p_{3/2}^N \rightarrow s_{1/2}^{\Lambda}$  transition leading to  $1_1^-$ , the spin-nonflip matrix element is large and the spin-flip one is small. On the other hand, the situation is opposite for the  $p_{1/2}^N \rightarrow s_{1/2}^{\Lambda}$  transition leading to  $1_2^-$ . Because the  $f$  amplitude is dominant at  $p_{\pi^+} \simeq 1$  GeV/c and  $\theta_K \simeq 15^\circ$  (cf. Fig. 8), a state with a larger share of the spin-nonflip transition has a larger cross section, and hence the  $1_1^-$  state is excited more strongly than  $1_2^-$ . Then the polarization becomes small (large) for the  $1_1^-$  ( $1_2^-$ ) state, since the product of the polarization and the cross section is proportional to the  $f$ - $g$  interference term,  $\sum_{M_f} \rho^{fg}(M_f)$ , and  $\rho^{fg}(M_f)$  itself does not differ so much between the  $1_1^-$  and  $1_2^-$  state.

Next, the reason is also remarked why  $P_H(2_1^+)$  is so much smaller than  $P_H(2_2^+)$  (0.07 vs  $-0.45$  at  $\theta_K = 10^\circ$ ), although both states are excited equally strongly (cf. Tables I and II). The  $2_1^+$  state having the structure

$$[\Phi({}^{11}\text{C}, \frac{3}{2}^-) \otimes p_{3/2}^{\Lambda}]_{2^+}$$

is excited mainly through the  $p_{3/2}^N \rightarrow p_{3/2}^{\Lambda}$  transition from the  ${}^{12}\text{C}$  target. However, the spin-flip  $g$  term does not contribute to this transition. This results from the kinematical reason in the Racah algebra. If the single-particle transition occurs from  $(n^N l^N j^N)$  to  $(n^{\Lambda} l^{\Lambda} j^{\Lambda})$  by keeping  $l^N = l^{\Lambda}$  and  $j^N = j^{\Lambda}$ , then the matrix element of the spin-flip operator

$$\langle n^{\Lambda} l^{\Lambda} j^{\Lambda} || \tilde{j}_{LM} [Y_L \times \sigma]_K || n^N l^N j^N \rangle = 0 \text{ if } K = L, \quad (13)$$

because the relevant 9- $j$  symbol vanishes. In the present case of  $0^+ \rightarrow 2^+$  transition, the angular momentum transfer  $K$  is 2. Thus the  $f$ - $g$  interference term of matrix elements becomes zero and the polarization vanishes for the dominant transition leading to the  $2_1^+$  state. On the other hand, the  $2_2^+$  state has a large polarization due

to the  $p_{3/2}^N \rightarrow p_{1/2}^{\Lambda}$  transition which has a large spin-flip contribution.

The final comment in this subsection is that the  $\Lambda$ -spin polarizations  $P_{\Lambda}(J_f)$  defined by Eq. (6) are always positive irrespective to the hypernuclear states (see triangles in the figures). The prediction reflects the positive sign of a  $\Lambda$  polarization in the elementary  $\pi^+ n \rightarrow \Lambda K^+$  process. Note here that many high-spin states in the quasifree region generally have large hypernuclear polarizations  $P_H(J_f)$  but their signs are state dependent. See Table II for the averaged  $P_{\Lambda}(\theta_K)$  in the continuum of  $15 < E_x < 35$  MeV.

For typical states in the bound region, we list the predictions:

$$P_{\Lambda}(1_1^-) = 0.19, \quad P_{\Lambda}(1_2^-) = 0.81,$$

and

$$P_{\Lambda}(2_2^+) = 0.21 \text{ at } \theta = 15^\circ.$$

See Table II for  $P_{\Lambda}$  estimated at other scattering angles.

## B. Polarizations in the ${}^{13}_{\Lambda}\text{C}$ production

Figure 3 (bottom) shows the hypernuclear polarizations (straight line) and the  $\Lambda$ -spin polarizations (open triangle) of  ${}^{13}_{\Lambda}\text{C}$  at  $\theta_L = 10^\circ$ . The three bound states,  $\frac{1}{2}^+$ ,  $\frac{3}{2}^+$ , and  $\frac{3}{2}^-$ , below the  $\Lambda$  and proton thresholds have large hypernuclear polarizations and at the same time the large  $\Lambda$ -spin polarizations. The values estimated at  $\theta_K = 10^\circ$  are

$$P_H(\frac{1}{2}^+) = 0.61, \quad P_H(\frac{3}{2}^+) = -0.25,$$

and

$$P_H(\frac{3}{2}^-) = 0.48.$$

Far larger polarizations are expected at  $\theta_K = 15^\circ$  as listed in Table II.

In the  $(\pi^+, K^+)$  reaction on the  ${}^{13}\text{C}(\frac{1}{2}^-)$  target, the ground  $\frac{1}{2}^+$  state is excited through the total angular momentum transfers  $K = 0$  and 1 with the orbital angular momentum transfer  $L = 1$  [cf. Eq. (13)]. The large and positive polarization of the ground  $\frac{1}{2}^+$  state is due to the  $p_{1/2}^N \rightarrow s_{1/2}^{\Lambda}$  single-particle transition in which the spin-

flip contribution ( $L = 1, S = 1, K = 1$ ) is comparable to the spin-nonflip one ( $L = 1, S = 0, K = 1$ ) and the  $f$ - $g$  interference produces the marked polarization. Note that the other component does not contribute to the  $\frac{1}{2}_1^+$  polarization.

On the other hand, the  $\frac{3}{2}_1^+$  state which is separated as much as 4.6 MeV from the ground state has negative and relatively small polarization. The  $\frac{3}{2}_1^+$  state is excited through the angular momentum transfer  $K = 1$  and 2 with  $L = 1$ . The  $p_{3/2}^N \rightarrow s_{1/2}^\Lambda$  single-particle transition is mainly responsible for the excitation of the  $\frac{3}{2}_1^+$  state, where the spin-nonflip contribution ( $L = 1, S = 0, K = 1$ ) is larger than the spin-flip one ( $L = 1, S = 1, K = 1$ ) and other components ( $K = 2$ ) give small contributions. Thus the relatively small polarization results with the different sign.

The  $\frac{3}{2}_1^-$  state at  $E_\Lambda^{\text{cal}} = -1.69$  MeV ( $E_x = 10.0$  MeV) is excited through the  $p_{1/2}^N \rightarrow p_{3/2}^\Lambda$  transition for which the spin-flip operator plays a more important role than the spin-nonflip one and hence the large polarization is obtained.

Figure 10 displays the angular dependence of the polarizations  $P_H$  for the three states discussed above. The polarizations increase monotonically with the angle and the amounts seem enough to be used in a possible coincidence experiment involving weak-decay particles. In addition, we point out that the sizable energy separations between these hypernuclear states are also favorable in view of practical feasibility.

### C. Polarizations in the ${}^{16}_\Lambda\text{O}$ production

Three distinct levels below the  $\Lambda$  threshold of  ${}^{16}_\Lambda\text{O}$  are seen to have sizable polarizations as displayed in Fig. 4 (bottom). The expected values at  $\theta_K = 10^\circ$  are

$$P_H(1_1^-) = 0.59, \quad P_H(1_2^-) = -0.28,$$

and

$$P_H(2_1^+) = 0.46$$

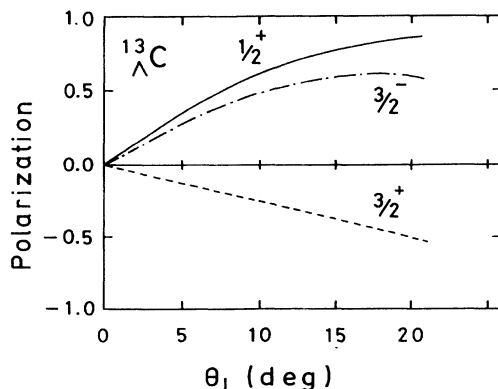


FIG. 10. The angular dependence of the hypernuclear polarization  $P_H(J)$  of  ${}^{13}_\Lambda\text{C}$  ( $J = \frac{1}{2}_1^+, \frac{3}{2}_1^+, \text{ and } \frac{3}{2}_1^-$ ) states as calculated in DWIA with the mixed wave functions.

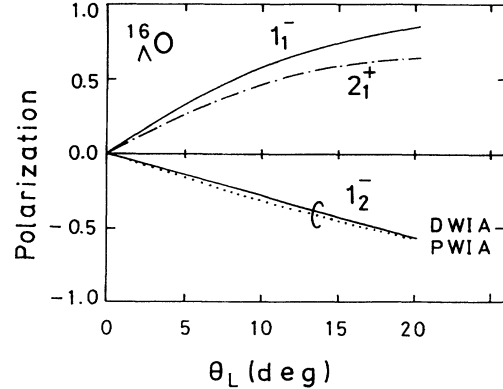


FIG. 11. The angular dependence of the hypernuclear polarization  $P_H(J)$  of  ${}^{16}_\Lambda\text{O}$  ( $J = 1_1^-, 1_2^-, \text{ and } 2_1^+$ ) states, as calculated in DWIA with the mixed wave functions. For comparison, the PWIA result is also shown by a dotted line for  $1_2^-$ .

for which the calculated excitation energies are listed in Table II together with the polarizations at other angles.

Starting from the  ${}^{16}_\Lambda\text{O}$  target, the transition leading to  $1_1^-$  ( $1_2^-$ ) in  ${}^{16}_\Lambda\text{O}$  follows the same mechanism as explained in Sec. IV A for the excitation of  $1_2^-$  ( $1_1^-$ ) in  ${}^{12}_\Lambda\text{C}$ —the  $p_{1/2}^N \rightarrow s_{1/2}^\Lambda$  transition prevails and the large polarization is induced for the ground  $1_1^-$  state, while the  $p_{3/2}^N \rightarrow s_{1/2}^\Lambda$  transition gives relatively small polarization for  $1_2^-$ . Note that the  $p_{1/2}$  neutron orbit is closed in the  ${}^{16}_\Lambda\text{O}$  target in place of  $p_{3/2}$  in the first approximation for  ${}^{12}_\Lambda\text{C}$ .

Even further analogies are recognized: the excitation of the  $2_1^+$  state of  ${}^{16}_\Lambda\text{O}$  from the  ${}^{16}_\Lambda\text{O}$  target is analogous to the excitation of the  $2_2^+$  state of  ${}^{12}_\Lambda\text{C}$  from the  ${}^{12}_\Lambda\text{C}$  target, where the former excitation is produced via the  $p_{1/2}^N \rightarrow p_{3/2}^\Lambda$  transition and the latter one via the  $p_{3/2}^N \rightarrow p_{1/2}^\Lambda$  transition. Both the  $1_1^-$  state and the  $2_1^+$  state have large  $\Lambda$ -spin polarizations. Those states, that are excited through the spin-flip transitions such as  $p_{1/2}^N \rightarrow s_{1/2}^\Lambda$ ,  $p_{3/2}^N \rightarrow p_{1/2}^\Lambda$ , and  $p_{1/2}^N \rightarrow p_{3/2}^\Lambda$ , can have large hypernuclear polarizations and large  $\Lambda$ -spin polarizations.

Figure 11 shows the angular dependence of the polarization  $P_H$  for these typical states in  ${}^{16}_\Lambda\text{O}$ . In order to demonstrate the meson-distortion effect, the polarization of the  $1_2^-$  state is evaluated in PWIA as well. In Fig. 11 one sees the effect is small and the spin-flip interaction is most responsible for the obtained polarization up to  $\theta_K \sim 20^\circ$ .

### D. Polarizations in the ${}^{10}_\Lambda\text{B}$ , ${}^{11}_\Lambda\text{B}$ , and ${}^{14}_\Lambda\text{N}$ productions

Based on the experimental  $\Lambda$ -binding energies, we expect the lowest threshold of  ${}^9_\Lambda\text{Be}+p$  at 2.0 MeV excitation. Therefore, among the particle-stable states in  ${}^{10}_\Lambda\text{B}$ , only the  $2_1^-$  member of the ground-state doublet has appreciable polarization as well as the sizable cross section (see Fig. 5):

$2_1^-(E_\Lambda^{\text{cal}} = -8.73 \text{ MeV}; E_x = 0.16 \text{ MeV}) :$

$$\frac{d\sigma}{d\Omega} = 2.86 \mu\text{b/sr}, \quad P_H = P_\Lambda = 0.31 \text{ at } \theta_K = 10^\circ.$$

This is due to the condition that the angular momentum transfer  $L = 1$  is allowed from the target ground state  $^{10}\text{B}(3^+)$  and the  $p_{3/2}^N \rightarrow s_{1/2}^\Lambda$  transition is possible. On the contrary, the spin-partner  $1^-$  has a very small cross section and negligible polarization because this state is excited only by the spin-flip interaction.

In  $^{11}_\Lambda\text{B}$  of Fig. 6, one sees that the ground  $\frac{5}{2}^+$  state is pronouncedly excited in the  $(\pi^+, K^+)$  reaction and the expected polarization is appreciable:

$$\frac{5}{2}_1^+(\text{g.s.}) : \frac{d\sigma}{d\Omega} = 4.05 \mu\text{b/sr}, \quad P_H = -0.24, \quad P_\Lambda = 0.17$$

at  $\theta_K = 10^\circ$ .

The level density in the bound state region is high and it seems unfavorable for an ordinary spectroscopic study with polarization measurement. However, the cross section summed over the particle-bound states amounts to  $13 \mu\text{b/sr}$  or more at  $\theta_K < 10^\circ$  and therefore the  $(\pi^+, K^+)$  production of  $^{11}_\Lambda\text{B}$  itself remains still meaningful to be used as a study of the weak decay. On the other hand, the polarized  $^{11}_\Lambda\text{B}$  states [29] can also be populated via the proton emission from the polarized excited states in  $^{12}\text{C}$  as has been already done experimentally [9].

The predicted polarizations in the  $^{14}_\Lambda\text{N}(\pi^+, K^+)^{14}_\Lambda\text{N}$  reaction are shown in Fig. 7. As the  $^{13}_\Lambda\text{C}+p$  threshold lies at 2.4 MeV excitation and the  $0^-$  member of the ground-state doublet has no polarization kinematically, the polarization of  $1_1^-$  is quite interesting. The predicted values are

$$1_1^-(\text{g.s.}) : \frac{d\sigma}{d\Omega} = 1.47 \mu\text{b/sr}, \quad P_H = P_\Lambda = 0.31$$

at  $\theta_K = 10^\circ$ .

Note that this value at the production stage does not acquire the depolarization effect due to the lack of  $\gamma$  cascades (Fig. 7). The present polarization is induced by the  $p_{1/2}^N \rightarrow s_{1/2}^\Lambda$  transition. It is noted, however, that the target nucleus  $^{14}\text{N}$  has spin  $J = 1^+$  and then the transition to  $^{14}_\Lambda\text{N}$  involves various angular momentum transfer  $K$  with contributions from both spin-flip and spin-nonflip single-particle transitions.

## V. CONCLUDING REMARKS

Starting with the spin-flip and spin-nonflip amplitudes,  $f + ig(\boldsymbol{\sigma} \cdot \hat{\mathbf{n}})$ , of the elementary  $\pi^+ n \rightarrow \Lambda K^+$  process, the hypernuclear production cross sections and polarizations have been evaluated in DWIA for the  $(\pi^+, K^+)$  reactions on available  $p$ -shell nuclear targets ( $^{10,11}\text{B}$ ,  $^{12,13}\text{C}$ ,  $^{14}\text{N}$ ,  $^{16}\text{O}$ ). First the use of the elementary amplitudes and the configuration-mixed hypernuclear wave functions yielded an improved treatment of the  $(\pi^+, K^+)$  excitation func-

tions and the angular distributions for typical states. Second we presented the refined estimates of hypernuclear polarizations as a whole and the  $\Lambda$ -spin polarization in nuclear medium.

The overall structures of the  $(\pi^+, K^+)$  experimental excitation spectra [16] of  $^{12}_\Lambda\text{C}$ ,  $^{13}_\Lambda\text{C}$ , and  $^{16}_\Lambda\text{O}$  are satisfactorily reproduced in the present calculations. The calculated cross sections and angular distributions for the typical peaks are in very good agreement with the experimental data reported from Brookhaven (and also from KEK for  $^{12}_\Lambda\text{C}$  [30]). In the refined framework it is also clarified that the previous treatment of using the formula  $\frac{d\sigma}{d\Omega} = \alpha(\frac{d\sigma}{d\Omega})_{\text{elem}} N_{\text{eff}}$ , thus neglecting the spin-flip interaction, works practically well as far as the production cross sections are concerned. Moreover, by using the configuration-mixed wave functions, we predict the detailed hypernuclear level structures in the excitation functions which should be tested to extract information on the  $\Lambda N$  interaction in improved experiments.

The novel feature of the present calculation with  $f$  and  $g$  amplitudes is to predict the hypernuclear polarization  $P_H(J)$  and the  $\Lambda$ -spin polarization  $P_\Lambda(J)$  in the production reaction. This provides wide possibility of coincidence experiments involving the polarizations such as asymmetry measurements of weak-decay protons and pions. The  $(\pi^+, K^+)$  reaction at  $p_\pi \simeq 1 \text{ GeV}/c$  induces large hypernuclear polarizations and large  $\Lambda$ -spin polarizations at the production stage. Among others, those natural parity states have been shown to be favored in the reaction that have both of the following two conditions: (i) the excitation through the nonzero orbital angular momentum transfer from the target and (ii) the excitation by the spin-flip transitions such as  $p_{3/2}^N \rightarrow s_{1/2}^\Lambda$ ,  $p_{1/2}^N \rightarrow s_{1/2}^\Lambda$ ,  $p_{3/2}^N \rightarrow p_{1/2}^\Lambda$ , and  $p_{1/2}^N \rightarrow p_{3/2}^\Lambda$ .

It is pointed out that the use of the mixed wave functions changes appreciably the previous estimate with the simple 1p-1h wave function for  $^{12}\text{C}$ . Here we list the typical states that are predicted to have sizable hypernuclear polarizations and  $\Lambda$ -spin polarizations at  $\theta_K \geq 10^\circ$ :

$$\begin{aligned} ^{10}_\Lambda\text{B} : & 2_1^-(E_x^{\text{cal}} = 0.16 \text{ MeV}), \\ ^{11}_\Lambda\text{B} : & \frac{2}{5}^+(\text{g.s.}), \\ ^{12}_\Lambda\text{C} : & 1_1^-(\text{g.s.}), 1_2^-(E_x^{\text{cal}} = 1.75 \text{ MeV}), \\ & \text{and } 2_2^+(10.61 \text{ MeV}), \\ ^{13}_\Lambda\text{C} : & \frac{1}{2}_1^+(\text{g.s.}), \frac{3}{2}_1^+(E_x^{\text{cal}} = 4.60 \text{ MeV}), \\ & \text{and } \frac{3}{1}^-(10.00 \text{ MeV}), \end{aligned}$$

$$\begin{aligned} ^{14}_\Lambda\text{N} : & 1_1^-(\text{g.s.}), \\ ^{16}_\Lambda\text{O} : & 1_1^-(\text{g.s.}), 1_2^-(E_x^{\text{cal}} = 6.23 \text{ MeV}), \\ & \text{and } 2_1^+(10.50 \text{ MeV}). \end{aligned}$$

In the quasifree region, nearly constant and positive

$\Lambda$ -spin polarizations are obtained for all the cases concerned. Although this feature is consistent with the  $\Lambda$  polarization in the elementary process, the predicted values  $\bar{P}_\Lambda \simeq 0.25\text{--}0.35$  ( $\theta_K = 10^\circ\text{--}15^\circ$ ) for the region  $15 \leq E_x < 35$  MeV are about 50% reduced from the free value. The theoretical values seem underestimated in view of the recent observation [9].

We separated the polarization of a hypernuclear state into two categories: the polarization at the production stage and the polarization at the weak decay stage. Here we confined ourselves to the former. However, the coincidence measurement of the weak-decay particles from the  $^{12}\text{C}(\pi^+, K^+)_{\Lambda}^{12}\text{C}$  reaction has been already performed at KEK [9]. For nonmesonic decays of  $_{\Lambda}^{12}\text{C}$  and  $_{\Lambda}^{11}\text{B}$ , the ECHO group deduced the proton asymmetry coefficients  $A_1$  which consist of the  $\Lambda$ -spin polarization and the intrinsic asymmetry parameter  $\alpha_1^{\text{NM}}$ . In order to make a realistic comparison with these data, it is necessary to estimate the modification effects due to particle and/or  $\gamma$  emissions to obtain the polarization just before the weak decay. In a subsequent paper [29] we will take such depolarization processes into account and discuss the modified ground-state polarizations in the light of hypernuclear weak decays.

## ACKNOWLEDGMENTS

This work started under the support from the Grant-in-Aid for Scientific Research (C) and also from the Grant under the Monbusho International Scientific Research program (Joint Research 1990–1991). Two of the authors (O.R. and M.S.) are indebted to the latter financial aid for the stay in Osaka. K.I. and T.M. are grateful to Professor R. Mach for his kind hospitality during their stay at the Nuclear Physics Institute in Rež/Prague. T.M. likes to express his thanks to the Institute for Nuclear Theory, University of Washington, for extending him hospitality during the Program-VIII (1992). We wish to thank H. Ejiri, T. Fukuda, O. Hashimoto, A. Higashi, T. Kishimoto, T. Nagae, and H. Noumi for discussions on the experimental results. This is also a part of the annual project on “Productions, Structures and Decays of Hypernuclei” of Yukawa Institute for Theoretical Physics, Kyoto University (1991–1992). Numerical calculations have been done at the Data Processing Center of Kyoto University under the financial support (in part) from the Research Center for Nuclear Physics, Osaka University.

- 
- [1] H. Bandō, T. Motoba, and J. Žofka, *Int. J. Mod. Phys. A* **5**, 4021 (1990).
  - [2] K. Itonaga, T. Motoba, O. Richter, M. Sotona, and J. Žofka, *Few-Body Systems Suppl.* **5**, 372 (1992); K. Itonaga *et al.*, *Nucl. Phys.* **A547**, 57c (1992). In these proceedings, a part of the present calculations has been reported briefly.
  - [3] A. Masaïke and H. Ejiri, in *Proceedings of the Third LAMPF II Workshop*, edited by J. C. Allred *et al.*, Los Alamos National Laboratory Report No. 9933-CII (Los Alamos, NM, 1983), p. 823.
  - [4] H. Bandō, *Genshikaku-Kenkyu* (INS, Tokyo) **31**, 99 (1986).
  - [5] H. Ejiri, T. Fukuda, T. Shibata, H. Bandō, and K.-I. Kubo, *Phys. Rev. C* **36**, 1435 (1987).
  - [6] R. D. Baker *et al.*, *Nucl. Phys.* **B141**, 29 (1987); **B126**, 365 (1977); D. H. Saxon *et al.*, *ibid.* **B162**, 522 (1980); K. W. Bell *et al.*, *ibid.* **B222**, 389 (1983).
  - [7] M. Sotona and J. Žofka, *Prog. Theor. Phys.* **81**, 160 (1989).
  - [8] H. Bandō, T. Motoba, M. Sotona, and J. Žofka, *Phys. Rev. C* **39**, 587 (1989).
  - [9] S. Ajimura *et al.*, *Nucl. Phys.* **A547**, 47c (1992); *Phys. Rev. Lett.* **68**, 2137 (1992); *Phys. Lett. B* **282**, 293 (1992).
  - [10] C. B. Dover, L. Ludeking, and G. E. Walker, *Phys. Rev. C* **22**, 2073 (1980).
  - [11] H. Bandō and T. Motoba, *Prog. Theor. Phys.* **76**, 1321 (1986).
  - [12] T. Motoba, H. Bandō, R. Wunsch, and J. Žofka, *Phys. Rev. C* **38**, 1322 (1988).
  - [13] R. Hausmann and W. Weise, *Nucl. Phys.* **A491**, 598 (1989).
  - [14] K. Itonaga, T. Motoba, and H. Bandō, *Prog. Theor. Phys.* **84**, 291 (1990).
  - [15] C. Milner *et al.*, *Phys. Rev. Lett.* **54**, 1237 (1985).
  - [16] R. E. Chrien, *Nucl. Phys.* **A478**, 705c (1988).
  - [17] P. H. Pile *et al.*, *Phys. Rev. Lett.* **66**, 2585 (1991).
  - [18] M. Akei *et al.*, *Nucl. Phys.* **A534**, 478 (1991).
  - [19] S. Cohen and D. Kurath, *Nucl. Phys.* **A101**, 1 (1967).
  - [20] Y. Yamamoto and H. Bandō, *Prog. Theor. Phys.* **73**, 905 (1985); *Prog. Theor. Phys. Suppl. No.* **81** (1985), Chap. II, p. 9.
  - [21] M. M. Nagels, T. A. Rijken, and J. J. deSwart, *Phys. Rev. D* **12**, 744 (1975); **15**, 2547 (1977); **20**, 1633 (1979).
  - [22] D. Ziemeńska and R. H. Dalitz, *Nucl. Phys.* **A238**, 453 (1975).
  - [23] D. Ziemeńska, *Nucl. Phys.* **A242**, 461 (1975).
  - [24] R. E. Chrien *et al.*, *Phys. Rev. C* **41**, 1062 (1990).
  - [25] O. Hashimoto, in *Perspectives in MESON SCIENCE*, edited by T. Yamazaki *et al.* (North-Holland, Amsterdam, 1992), Chap. 9, p. 547.
  - [26] A. Bouyssy, *Nucl. Phys.* **A290**, 324 (1977); *Phys. Lett.* **91B**, 15 (1980).
  - [27] W. Brückner *et al.*, *Phys. Lett.* **79B**, 157 (1976).
  - [28] M. May *et al.*, *Phys. Rev. Lett.* **47**, 1106 (1981).
  - [29] K. Itonaga *et al.* (unpublished).
  - [30] O. Hashimoto (private communication); T. Nagae, talk at the Particles and Nuclei International Conference (PANIC), Perugia, Italy, 1993 (unpublished).